Permanent stiffness reduction by thermal oxidation of silicon

Kuppens, Reinier; Herder, Just; Tolou, Nima

DOI
10.1109/JMEMS.2019.2935379

Publication date
2019

Document Version
Final published version

Published in
Journal of Microelectromechanical Systems

Permanent Stiffness Reduction by Thermal Oxidation of Silicon

P. Reinier Kuppens, Just L. Herder, *Member, IEEE*, and Nima Tolou

***Abstract*— Stiffness in compliant micro mechanisms can negatively affect performance. Current methods for stiffness reduction in micro electro mechanical systems (MEMS) consume power, have a large footprint or are relatively complex to manufacture. In this paper stiffness is reduced by static balancing. A building block commonly used for stiffness reduction in large scale compliant mechanisms is made compatible with MEMS. Preloading required to create negative stiffness is obtained from residual film stress by thermal oxidation of silicon. Instead of buckling a plate spring by moving its end points, a SiO_2 film 1900 nm to 2500 nm thick will stretch micro-beams 24 µm wide, while the end points are fixed. To show efficacy of our method, the building block is coupled with a simple linear stage. However, the building block can readily be combined with other compliant micro mechanisms to reduce their stiffness. Statically balanced MEMS will enable novel designs in low-frequency sensor technology, low-frequency energy harvesting and pave the way to autonomous micro-robotics. We show a stiffness reduction of a factor 9 to 46. The balancing effect remained after SiO_2 removal, due to plastic deformation of the beams. [2019-0023]**

***Index Terms*— Compliant mechanisms, MEMS, static balancing, stiffness reduction, thin films, silicon, thermal oxidation.**

I. Introduction

COMPLIANT mechanisms (CM) move due to deformation of slender segments. They are a necessity rather than a design choice for micro electro mechanical systems (MEMS), because CMs can be monolithic [1] and assembly is economically unjustifyable [2]. Even though CMs have many advantages over conventional mechanisms (e.g. increased precision, increased reliability, reduced wear and simplified manufacturing [3]) a disadvantage is that they store a significant part of the input energy as strain energy due to stiffness [4]. This may affect the input-output relation with an insufficient travel range, a low energy efficiency and a high natural frequency [5], [6].

Stiffness in MEMS can be reduced by active methods such as electrostatic actuation, piezo electric acutation and joule heating [7]. However, these methods consume power, have a large footprint and manufacturing complexity is relatively high. A passive alternative is static balancing (SB) [6].

Manuscript received February 7, 2019; revised July 26, 2019; accepted July 29, 2019. Date of publication September 2, 2019; date of current version October 1, 2019. This work was supported by the Research Institute of TAG Heuer, Branch of LVMH Swiss Manufacture. Subject Editor G. Stemme. *(Corresponding author: P. Reinier Kuppens.)*

The authors are with the Department of Precision and Microsystems Engineering, Faculty of Mechanical Engineering, Delft University of Technology (TU Delft), 2628 CD Delft, The Netherlands (e-mail: p.r.kuppens@tudelft.nl).

Color versions of one or more of the figures in this article are available online at http://ieeexplore.ieee.org.

Digital Object Identifier 10.1109/JMEMS.2019.2935379

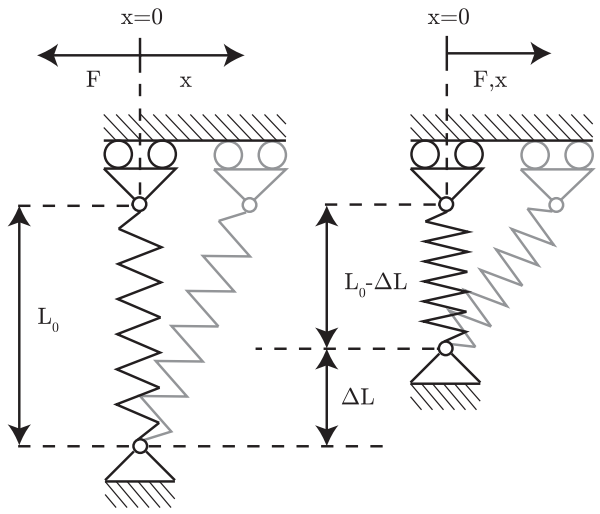

Fig. 1. Balancer with negative stiffness used for static balancing, comprised of a compression spring with free length L_0 on a cart. In the unloaded configuration (left), displacement of the cart results in a returning force to the stable equilibrium at $x = 0$. If preloaded a distance ΔL, displacement of the cart results in a force away from the unstable equilibrium at $x = 0$, i.e. negative stiffness.

In a statically balanced system the potential energy is kept constant over the entire range of motion, instead of in just one or multiple positions [8]. A balancer (e.g. the mechanism in Fig. 1) is responsible for counteracting all elastic forces generated by the functional mechanism, ensuring a sustained static equilibrium. It is essentially a mechanisms with opposing (negative) stiffness in parallel to a functional mechanism.

Negative stiffness (NS) mechanisms may have different forms [9]–[12], but they all require some kind of embedded potential energy. An inverted pendulum for example, requires to be put upright. Compliant mechanisms with negative stiffness, require flexible elements to be preloaded in postbuckling [13].

Preloading in large scale CMs is relatively straightforward by displacing the end points of plate springs. Literature shows plenty of examples [14]–[18]. However, preloading on micro-scale becomes a significant challenge since physical handling of micro structures with high precision and without causing damage is difficult [19]. Even though several concepts have been developed to circumvent preloading assembly, no methods are available for introducing the required potential energy to move the device into the statically balanced domain [19]–[21].

Statically balanced compliant micro mechanisms may find applications in low-frequency sensor technology [22], [23], low-frequency energy harvesting devices [24], [25] or compliant micro transmission mechanisms [26]. In addition they may revolutionize micro-robotics, because actuators do not have to overcome self-stiffness or the stiffness of the underlying kinematic structure. This would relax the energy requirements and pave the way to their autonomy. Applications of these robots in minimally invasive medicine are widespread [27].

In this paper a commonly used balancing building block [15] is made compatible with MEMS and their manufacturing techniques. We do so by stretching a silicon plate spring while keeping the endpoints fixed, instead of displacing the endpoints. The stretching is achieved by thermally growing a thin film of silicon dioxide on the silicon micro mechanism.

Thin films usually contain residual stresses. The film tends to expand if this stress is compresive and tends to shrink for a tensile stress [28]. Any film containing compressive residual stress will induce a tensile stress in the silicon substrate and stretch it. Surface stress has been suggested for removing inter component clearance and preloading [29] and is known to change the natural frequency of cantilever and doubly clamped micro-beams [30]–[32]. However, it has never been used to create a building block for statically balancing compliant micro mechanisms.

The MEMS balancing building block could be used to balance any sort of MEMS structure, such as a gripper [15], [16] or a rotational mechanism [14]. In this paper we introduce our method by balancing a simple linear stage. A balanced and unbalanced stage are compared to show efficacy.

The method is compatible with semi-conductor batch manufacturing techniques, enabling mass fabrication. It consumes no power after manufacturing, has a low manufacturing complexity and has a high resolution by controlling the film thickness. The equations of motion of a beam show that our method is theoretically able to reduce stiffness to zero [33]. And it has the potential to be 100% space efficient if positive and negative stiffness mechanisms are united in a single structure.

In Section II the stiffness reduction method is explained followed by an implementation in Section III. Manufacturing is explained in Section IV and simulations are discussed in Section V. How measurements are done is given in Section VI followed by the measurement results in Section VII. The implications of the results are discussed in Section VIII followed by a conclusion in Section IX.

II. Stiffness Reduction Method

The positive stiffness K_p of a CM can be reduced by coupling it with a mechanism with opposing negative stiffness K_n in parallel. The resulting equivalent stiffness is given by $K_{eq} = K_p + K_n$ and is zero if K_p and K_n are equal but opposite. These zero-stiffness compliant mechanisms are referred to as statically balanced [13].

Various negative stiffness mechanisms exist [9], [10], [15] that can be used as building blocks to balance an existing design [15]. One of the simplest is schematically shown in Fig. 1. In this mechanism a compression spring with a free length L_0 is preloaded a distance ΔL, causing instability around $x = 0$.

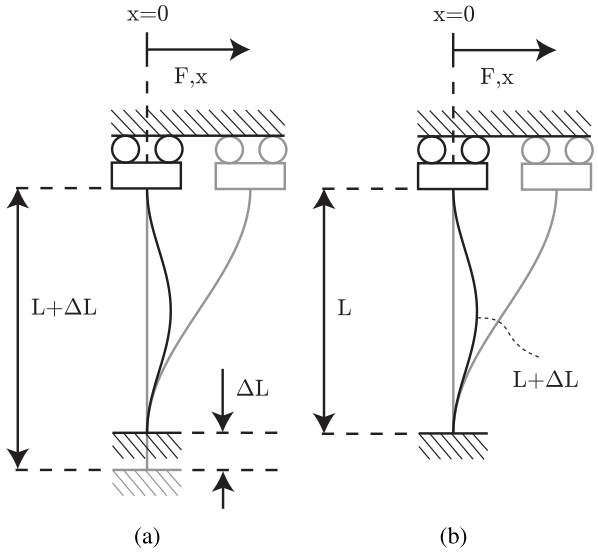

Fig. 2. Commonly used compliant equivalent of the balancer from Fig. 1. (a) Shows preloading by moving the end point of the plate spring a distance ΔL. (b) Shows preloading by stretching the plate spring a distance ΔL. Both systems are equivalent.

A commonly used compliant equivalent is shown in Fig. 2a. It is obtained by axially preloading a plate spring into its post-buckled state. Normally, the plate spring is preloaded by moving its endpoint an amount ΔL as shown in Fig. 2a [10], [12], [14]–[16]. An alternative, yet equivalent approach, is to elongate the plate spring an amount ΔL, as shown in Fig 2b.

We elongate the plate springs by uniformly depositing a thin film all around the silicon micro CM. Thin films virtually always contain residual stress, typically in the order of GPa [34]. They tend to expand if stress is compressive and tend to shrink for tensile stress [28].

In a freestanding substrate with a homogeneous thin film, the stress distribution follows from equilibrium of the normal forces and bending moments over the entire cross-section. Consequently, stress at the interface between film and substrate reverses sign and is small if the film thickness is small compared to substrate thickness [35]. If the film is in compression it will induce tension in the substrate. Hence, if the film is substantially thick, it will stretch the substrate. To prevent bending, the film should be applied uniformly around the substrate. This way all induced moments cancel each other.

Generally speaking, large stresses should be avoided in thin films, because they can lead to cracking or buckling of the film itself. One typically aims to get a compressive stress in the order of a few hundred MPa [28].

A. Minimum Required Film Stress

The total residual film stress σ_f is a combination of intrinsic σ_I and thermal σ_T stress:

$$\sigma_f = \sigma_I + \sigma_T \tag{1}$$

Intrinsic stress σ_I is generally hard to predict due to dependency on processing parameters [36]. For example, the stress in sputtered thin films is dependent on gas pressure, substrate bias, gas atomic mass, target atomic mass, angle of deposition, angle of emission, target shape and cathode power [37].

Thermal stresses σ_T are caused by a mismatch in the coefficient of thermal expansion (CTE) between the bulk and film materials. It is well understood and easily calculated with the following equation:

$$\sigma_f(T) = \left(\alpha_b - \alpha_f\right) \Delta T \frac{E_f}{1 - \upsilon_f} \tag{2}$$

where α_s and α_f are the CTE of the bulk and film material respectively, ΔT is the temperature difference and E_f and υ_f are the Youngs modulus and poisons ratio of the film.

In doubly-clamped beams film stress induces a net axial force [32]. It is given by the integral of the resulting axial stress over the beam cross-section. If the axial stress is due to a thin film only, this amounts to the integral of the stress in the thin film only [32]:

$$F_{axial} = \int_{A_f} \sigma_f dA \tag{3}$$

where F_{axial} is the net axial force, σ_f is a uniform strain-independent film stress and A_f is the cross sectional area of the thin film.

At sufficiently large axial loading the natural frequency of a beam becomes zero. This load can be derived from its dynamic equations and is called the Euler buckling load F_{cr} [33], [38]–[40]. For loads greater than F_{cr} the natural frequency becomes complex and the mode shape unstable [38], i.e. the beam buckles. For uniform beams under constant axial loading the Euler buckling load is given by:

$$F_{cr} = \frac{\pi^2 EI}{(KL)^2} \tag{4}$$

where E is the Youngs modulus, I is the surface moment of inertia, L is the length of the beam (see Fig. 2) and K is the effective length factor that depends on the boundary conditions. For a doubly-clamped beam $K = 0.5$ [38].

By equating Eq. 3 and Eq. 4 we can get the surface stress σ_{cr} that would cause the critical load:

$$\int_A \sigma_{cr} dA_f = \frac{\pi^2 EI}{(KL)^2} \tag{5}$$

Assuming a uniform thin film of thickness t that is negligible compared to the bulk of a beam of width b and height h (as definded in Fig. 4c) and a constant film stress σ_{cr} we get:

$$\sigma_{cr}\left(2bt + 2ht + 4t^2\right) = \frac{\pi^2 EI}{(KL)^2} \tag{6}$$

such that the critical film stress σ_{cr} becomes:

$$\sigma_{cr} = \frac{\pi^2 EI}{\left(2bt + 2ht + 4t^2\right)(KL)^2} \tag{7}$$

Material properties of silicon according to [41] are substituted in Eq. 7 along with a beam height $h = 525$ µm and a film thickness $t = 1.9$ µm. This yields a function for the critical stress σ_{cr} required for buckling a beam of width b and length L. It is plotted for various beam lengths in Fig. 3. It shows that thermally grown oxide can easily buckle silicon beams with lengths in the order of millimeters and a thickness in the order of tens of micrometers.

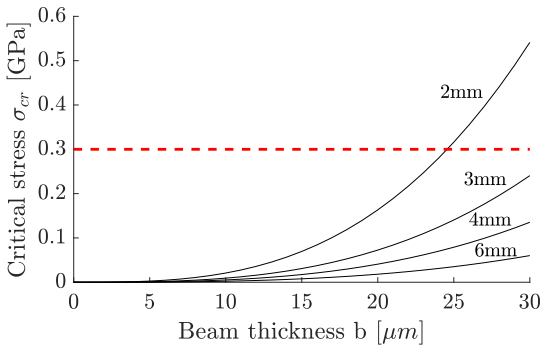

Fig. 3. Required critical stress according to Eq. 7 versus beam widths b for various beam lengths L. The dashed line indicates the maximum reported residual film stress in thermal oxide.

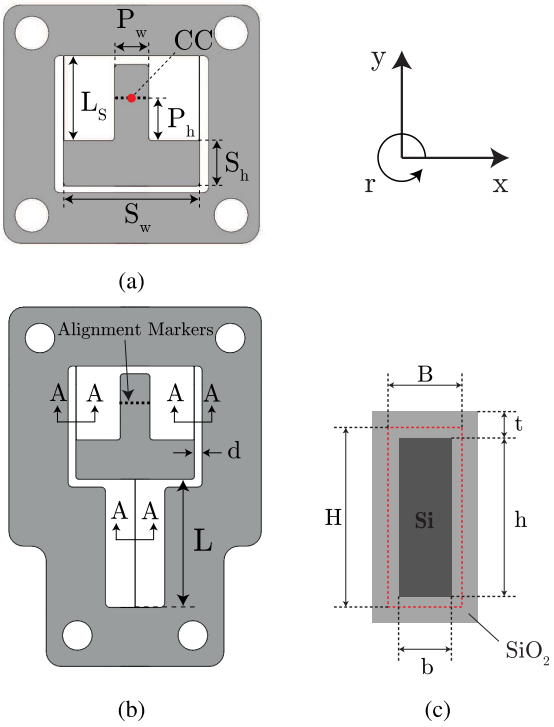

Fig. 4. Stage designs. (a) Shows the unbalanced stage and (b) the balanced stage. (c) Shows the cross section A-A of the plate springs, which is the same everywhere. The dashed rectangle indicates the silicon beam before some of its material is consumed by oxidation.

III. Mechanism Design

To demonstrate our stiffness reduction method the negative stiffness building block from Fig. 2b is placed in parallel with a linear stage, see Fig. 4. Although it could be combined with other mechanisms, see [14]–[16], this linear stage is arguably the simplest. The design goal is to reduce the stiffness of the stage from Fig. 4a as much as possible.

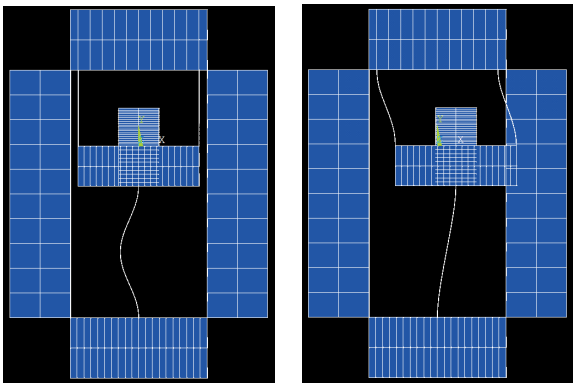

(a) Buckling mode shape 1 (b) Buckling mode shape 2

Fig. 5. The first two buckling modes resulting from uniformly cooling down the sample. Modeling is done as described in Section V.

Minimal stiffness is achieved by choosing the length L of the negative stiffness plate spring such that the critical loads (similar to F_{cr}) of the first two buckling modes (see Fig. 5) are the same. The critical load, induced by the film stress, is the load at which the system loses stability and its state bifurcates, i.e. the system can buckle left or right. The buckling modes give the shape in which the system will buckle. The modes and critical load can be computed with a linear buckling analysis (i.e. a linearized eigenvalue analysis) in any commercially available finite element program.

The residual stress in the SiO_2 will cause deformation in the shape of mode 1 or mode 2 (see Fig. 5) for large and small values of L respectively. However, for a particular value of L mode 1 and 2 can theoretically coexist, because they have the same critical load. Essentially, post buckling happens in the shape of mode 1 and 2 simultaneously, i.e. some linear combination of the eigenvectors associated with modeshape 1 and 2. This means that we can move the system from mode shape 1 to mode shape 2 without changing the potential energy in the system, which means the system is zero stiffness.

In practice, the buckling modes will always be slightly separated, i.e. their critical loads are slightly different. This is affected by modeling errors and by manufacturing tolerances caused by for example overetching or underetching of silicon. Consequently the structure will always buckle in either mode 1 or mode 2. A system buckled in mode 1 will have a reduced stiffness. However if the system is buckled in mode 2 it should be bistable [12], [42].

The length of the negative stiffness plate spring is $L = 8.673\,\text{mm}$ and the plate springs of the stage are chosen to have a length of $L_S = 5\,\text{mm}$. Please note that although the two plate springs of the stage are also stretched, they do not create any negative stiffness, because that would require them to buckle as shown in Fig. 2.

All plate springs have the same cross section A-A as shown in Fig. 4b and Fig. 4c. The width and height before oxidation are respectively $B = 24\,\mu\text{m}$ and $H = 525\,\mu\text{m}$ (wafer thickness). In practice B and H are slightly different from b and h, because some silicon is consumed during oxidation.

The shuttle is $S_w = 8\,\text{mm}$ wide and $S_h = 2.67\,\text{mm}$ high. It has a protrusion $P_w = 2\,\text{mm}$ wide with markers at height $P_h = 2.5\,\text{mm}$. It enables us to measure force and displacement close to the center of compliance (CC). At our CC all orthogonal compliance components are fully decoupled, which ensures no parasitic motions (e.g. r and y directions in Fig. 4) are induced during loading in the desired motion direction (x-direction) [43]. The markers are added to optically align the sensor probe with the mechanism, see Fig. 4b.

IV. Manufacturing

All mechanisms will be produced with DRIE and wet oxidation at 1100 °C from (100) oriented 525 µm thick silicon wafers. different oxide thicknesses are grown, 1.9 µm, 2.05 µm, 2.2 µm, 2.35 µm and 2.5 µm and 2.5 µm on five different wafers. Oxidation times are determined with the Deal-grove model [44] and thickness is across the front side of the wafer with spectral reflectance using a Leitz MPV SP. Wafers are oriented vertically in the oven to ensure uniform film growth on the front and back side. Before oxidation, one unbalanced stage is removed from each wafer.

Unbalanced linear stages with and without SiO_2 are manufactured and measured to determine the positive stiffness K_p to compensate. The balanced mechanisms with SiO_2 film are measured and compared with the unbalanced stiffness. In addition we remove the SiO_2 from the balanced mechanisms to investigate plastic effects of thermal oxidation on the Si beams. The SiO_2 is removed with a HF vapor etch using a SPTS Primaxx uEtch.

V. Simulations

Numerical modeling is done with ANSYS. Beam elements (beam188) with a custom trapezoidal cross sectional area are used. In case thin film is modeled a multi material (Si and SiO_2) cross section is defined as shown in Fig. 4. In case no thin film is modeled, a single material (Si) is defined. For the frame the effect of film stress is neglected, so a single material (Si) cross section is used. The frame is constrained in all directions to the ground at one corner.

The mono-crystalline silicon is assumed to be perfectly elastic. A constant orthotropic stiffness is used according to [41]. Which is equivalent to aligning all beams with the [010] crystal direction on the wafer, i.e. a 45 degree rotation with respect to the flat end. A temperature dependent CTE is used according to [45].

The reported material properties of thermally grown SiO_2 vary greatly [46]. Reported values for the CTE of silicon dioxide typically range from $0.5 \times 10^{-6}\,°\text{C}^{-1}$ to values as high as $4.1 \times 10^{-6}\,°\text{C}^{-1}$ [47]. And even negative values are reported. Youngs moduli range from 50 to 100 GPa and Poisson's ratios between 0.15 and 0.20 [46]. We have adopted elastic properties ($E = 72$ GPa, $\upsilon = 0.2$) from [48], where conditions are relatively comparable and are similar to data from [49]. A constant CTE of $0.5 \times 10^{-6}\,°\text{C}^{-1}$ is used as reported by [49]. Volume expansion during growth is accounted for by regarding the ratio of the atomic volume between Si and SiO_2, i.e. 20 Å to 40 Å [50].

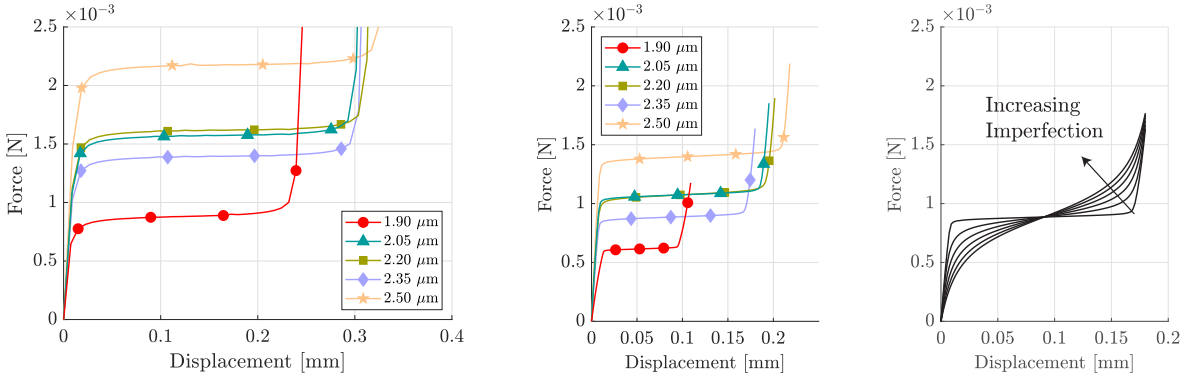

Fig. 6. Simulation results for statically balanced stages (a) with (b) and without oxide for multiple oxide thicknesses. (c) Shows the influence of beam imperfections on the force deflection response for the stage where 2.35 µm of SiO_2 has been removed.

A linear buckling analysis to compute the buckling shape modes and critical loads is performed by cooling down the material 1 °C. All elements are given an initial reference temperature of 970 °C (the viscous flow point of SiO_2) and a final uniform temperature of 969 °C to all nodes.

Modeling of the force deflection behaviour is done by a nonlinear static structural analysis. Again all elements are given an initial temperature of 970 °C, but are now given a final uniform temperature of 20 °C to model the cooling down to room temperature. Although plasticity of Si is observed in the measurements of the balanced stages, we do not predict and model plastic behaviour. Instead, we determine how much the neutral position has moved in the x-direction by measuring the distance d (see Fig. 4b) after oxide has been removed with a scanning electron microscope (SEM). It equals 55.10 µm, 98.59 µm, 101.80 µm, 90.86 µm and 110.14 µm for a film thickness of 1.9 µm to 2.5 µm respectively.

It is assumed the new equilibrium is stress free (without SiO_2) and that it has the shape of mode 2. Therefore we add buckling shape mode 2 with appropriate amplitude (distance d) to the original and undeformed neutral position. A uniform temperature of 20 °C is set to all nodes to model the cooling down of the sample. Force deflection behaviour is determined by computing reaction forces at regular intervals in the x-direction at the center of compliance.

Simulations are done for the balanced and unbalanced stages, both with and without oxide. The unbalanced stages with and without SiO_2 do not require any buckling modes to be added and are shown in Fig. 10b and Fig. 10a respectively. The balanced stages with and without oxide are shown in Fig. 6a and Fig. 6b respectively. Stiffness data is summarized in Tab. III.

Since the beams are not perfectly straight in practice, we model the influence of such defects by introducing geometric imperfections. Imperfections are simulated by adding the first three buckling modes with increasing amplitude to the undeformed nodal coordinates. That is, the sum of the first three buckling modes (at the new equilibrium) is scaled such that the maximum sideways deviation of the beams is 0 µm, 4 µm, 8 µm, 12 µm, 16 µm and 20 µm. We do this only for the simulations of the balanced stage with film thickness 2.35 µm. Results are shown in Fig. 6c.

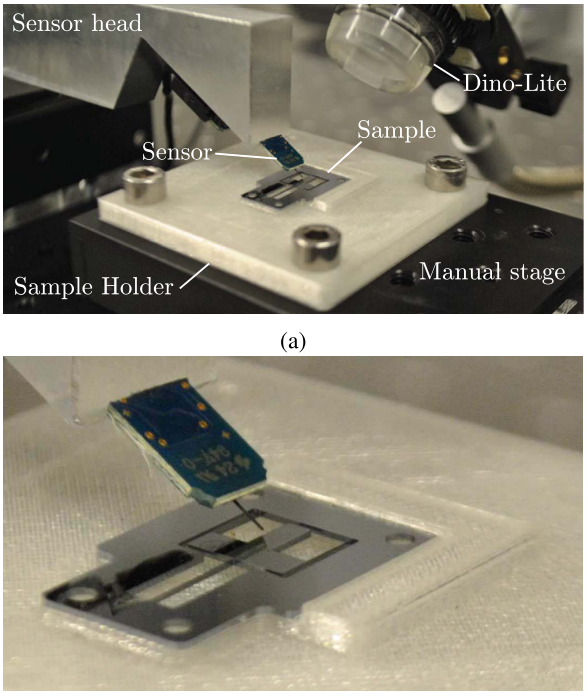

Fig. 7. Picture of the force deflection measurement setup. (a) Shows a closeup of the stage, sensor holder and digital microscope. (b) Shows a closeup of the microforce sensing probe and a sample.

VI. Measurements

Stiffness is analyzed in the x-direction of each stage by measuring the force deflection behavior. For this a microforce sensing probe (FT-S10000) with a resolution of 0.5 μN is mounted on a precision linear stage (Physik Instrumente M-060.2DG) with a resolution of 8.5 nm. The sensor is mounted under an angle of 30 degrees with an aluminum sensor head and vertically aligned using a manual linear precision stage (Thorlabs PT1). Samples are placed on a 3D printed

TABLE I

SiO_2 THICKNESS PER WAFER IN nm

Target	Bottom	Right	Top	Left	Center
1900 nm	1892	1891	1890	1889	1886
2050 nm	2050	2050	2052	2050	2048
2200 nm	2189	2187	2191	2192	2185
2350 nm	2352	2351	2349	2350	2349
2500 nm	2506	2506	2511	2511	2503

TABLE II

MEASURED AVERAGE FRONT AND BACK BEAM WIDTH IN µm FOR THE UNBALANCED STAGE (SU) AND BALANCED STAGE (SB) WITHOUT SiO_2. NOTE THAT SU IS NEVER OXIDIZED

	Back		Front	
Thickness	SU	SB - SiO_2	SU	SB - SiO_2
1900 nm	20.60	19.01	24.94	22.29
2050 nm	20.30	19.30	25.31	22.42
2200 nm	20.82	19.44	25.44	22.65
2350 nm	21.60	19.04	23.15	21.28
2500 nm	23.94	21.47	25.87	22.40

TABLE III

SIMULATED STIFFNESS IN N m^{-1} FOR THE UNBALANCED STAGE (SU) AND BALANCED STAGE (SB) WITH AND WITHOUT OXIDE

Thickness	SU	SU + SiO_2	SB + SiO_2	SB
1900 nm	13.02	13.65	0.29	0.27
2050 nm	13.13	13.77	0.18	0.32
2200 nm	13.67	14.45	0.17	0.42
2350 nm	12.27	13.40	0.16	0.30
2500 nm	16.92	18.35	0.17	0.37

L-shaped base plate and positioned using two manual linear precision stages. A picture of the measurement setup is shown in Fig. 7.

The sensing probe is visually aligned with the alignment markers at the CC and vertically halfway the thickness by using a Dino-Lite digital microscope and the manual precision stages. All measurements are averaged over 10 repetitions to reduce constant measurement noise, see Fig. 10.

Beam thickness is measured by using a low vacuum SEM. In one device all beams are measured in three locations on the front and back to get an idea of the distribution. In all other devices the average is taken of two beams, measured in one location on front and back. For beam measurements of the unbalanced stages, devices that were never oxidized are used. For the balanced stages, oxide is first removed.

VII. MEASUREMENT RESULTS

Pictures of the unbalanced and the balanced stages are shown in Fig. 8a and Fig. 8b respectively. Measurements of the SiO_2 thickness are given in Tab. I. Film thickness on average varies -0.28 ± 4.13 nm from target thickness and are in agreement with expected values.

Measurements of beam width on the front and back side are reported in Tab. II. A typical SEM measurement is shown in Fig. 9c. Measurements on the front and back side had a variation of 0.11 µm and 0.32 µm respectively.

TABLE IV

MEASURED STIFFNESS IN N m^{-1} OF THE UNBALANCED STAGE (SU) AND THE BALANCED STAGE (SB) WITH AND WITHOUT OXIDE

Thickness	SU	SU + SiO_2	SB + SiO_2	SB
1900 nm	13.42	13.73	0.66	0.51
2050 nm	12.83	13.72	0.60	0.41
2200 nm	13.21	13.81	0.70	0.49
2350 nm	13.23	14.63	1.53	1.07
2500 nm	14.92	15.19	0.60	0.32

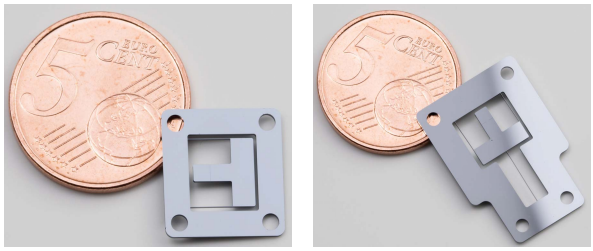

(a) (b)

Fig. 8. Manufactured stages. (a) Shows the unbalanced stage and (b) shows the balanced stage.

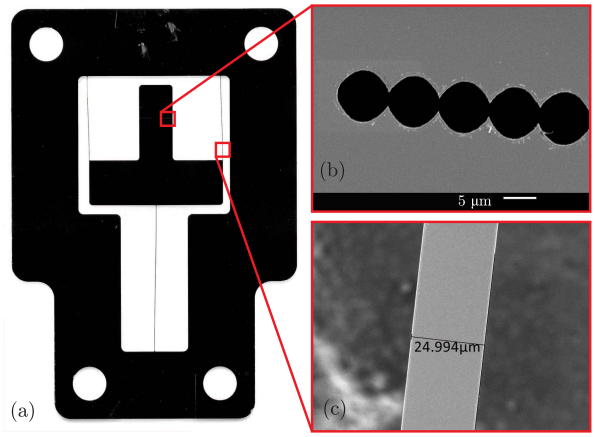

Fig. 9. Micrographs of a balanced stage. (a) A picture of a balanced stage. It can be observed it is buckled in the mode from Fig. 5b. (b) A SEM image of the markers used to align the microforce sensing probe with the center of compliance, see Fig. 4b. In figure (c) a typical SEM image used for measuring the beam width is shown.

Fig. 9a shows that the balanced device is buckled in mode shape 2 from Fig. 5b. Fig. 9b shows a SEM image of the alignment markers at the CC.

Force deflection measurements are shown in Fig. 10 and stiffness is summarized for all measurements in Tab. IV. Fig. 10a shows measurement data for one stage with SiO_2, including the linear fit and simulation results. Fig. 10b shows the same for one stage without 1.9 µm SiO_2. Measurements are in good agreement with simulations and stiffness increases 0.694 ± 0.47 N m^{-1} on average when oxidized.

Measurement results of the balanced stages with oxide present and after it has been removed are given in Sections VII-A and VII-B respectively.

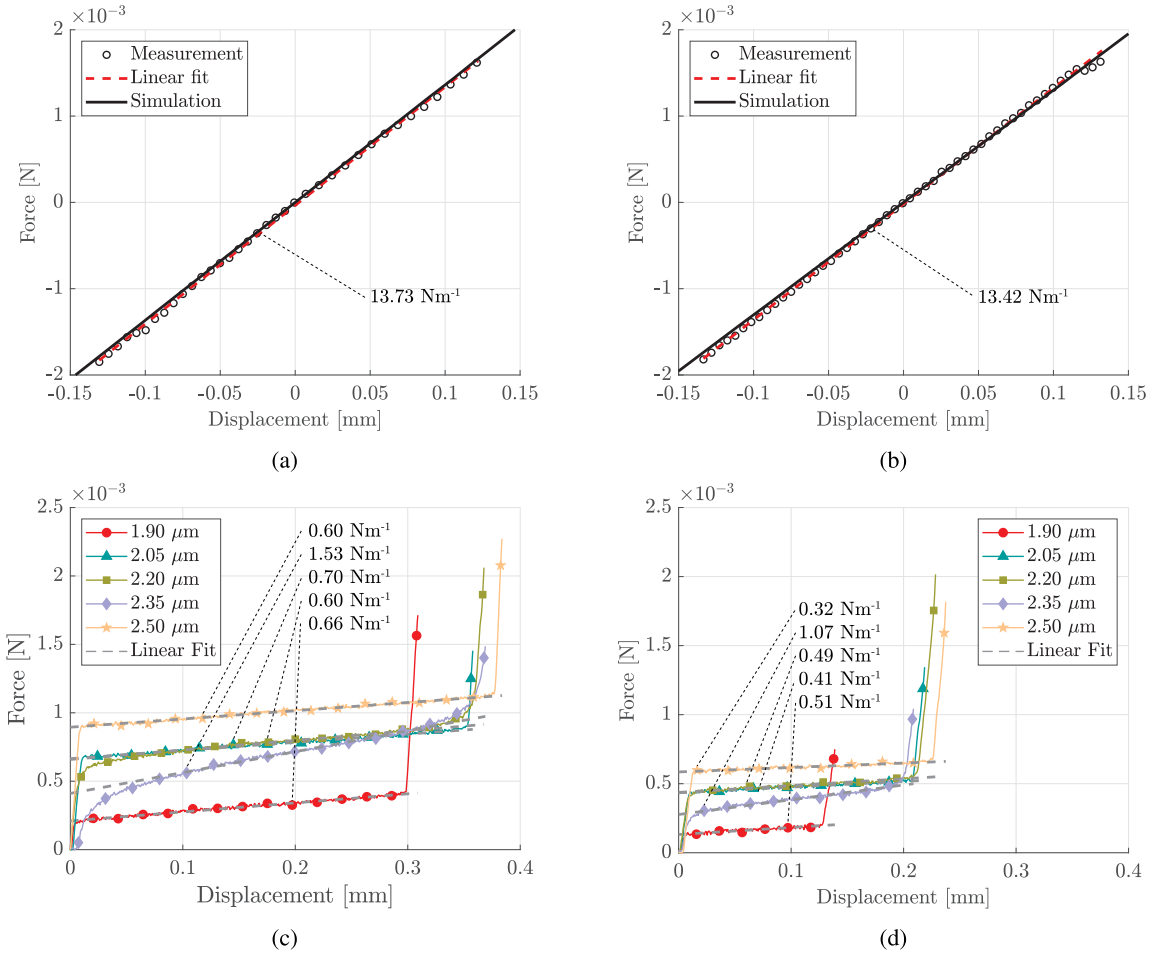

Fig. 10. Force deflection measurements averaged over 10 repetitions to reduce constant measurement noise. (a) A typical measurement with linear fit along with a simulation of an unbalanced oxidized stage. (b) A typical measurement with linear fit along with a simulation of a non-oxidized unbalanced stage. (c) Measurements of the balanced devices with SiO_2 with a linear fit to the low stiffness domain. (d) Measurements of the balanced devices with SiO_2 removed with a linear fit to the low stiffness domain.

A. Balance With Oxide

Fig. 10c shows all force deflection measurements for the balanced stages for all SiO_2 thicknesses. Fig. 10c also includes a linear fit to the low stiffness plateau. A clear reduction in stiffness can be observed compared to the non-balanced stages over a range of approximately 300 µm to 380 µm. The linear fit reveals a stiffness reduction of approximately a factor 9 to 25 compared to the unbalanced non-oxidized stage.

The low stiffness range increases for thicker films, but it also increases a constant force offset from approximately 0.2×10^{-3} N to 0.9×10^{-3} N, which can be explained by an increased change in neutral position, see Sec. VII-B. In addition it is remarkable that the curve of the balance stage with 2.35 µm SiO_2 is more rounded. It is likely that the beams in this mechanisms are less straight than in the other mechanisms, because Fig. 6c shows that with increasing beam imperfections the force deflection behaviour becomes more curvy.

B. Balance Without Oxide

Surprisingly, the balancing effect remained after oxide removal. Force deflection data, along with a linear curve fit, is shown in Fig. 10d. The linear fit reveals a stiffness reduction of approximately a factor 12 to 46 compared to the unbalanced non-oxidized stage. Almost half the stiffness of the balanced stages with SiO_2.

After oxide removal the balancing effect should completely disappear under purely elastic deformations. The remaining effect and the asymmetrical stiffness profiles (they are not centered around displacement 0 mm) in Fig. 10c and in Fig. 10d suggest irreversible plastic deformations in the silicon beams. That is, the oxidation process has permanently stretched the silicon beams, causing the post-buckling state to become the new equilibrium. However, stresses were not fully relaxed by plastic yielding, since the balancing domain and the force offset decreased upon oxide removal.

This shift in neutral position also explains the constant force offset, because it adds positive stiffness to the originally bistable mechanism. If bistability is combined with positive stiffness, a constant force mechanisms results [51]. The constant force offset increases for thicker films, because the severity of the bistability is increased for larger rotations of the plate springs. A parameter study of such a constant force mechanism can be found in [51].

VIII. Discussion

In this paper we have demonstrated, for the first time, one-time preloading for permanent stiffness reduction of flexible mechanisms at micro scale. A static balancing building block is made compatible with MEMS by exploiting residual stress from thermal oxidation of silicon. Efficacy is shown by coupling the building block to a simple linear stage, however it can be combined with other mechanisms as well [14]–[16].

The mechanism is unintentionally buckled in shape mode 2 instead of shape mode 1. Tolerances in manufacturing, caused by for example overetching or underetching of silicon, most likely changed the length and width of the beams causing a separation of the buckling modes with preference for mode shape 2. Sideways buckling may be prevented by properly separating the buckling modes, accounting for manufacturing tolerances. Ensuring the buckling shape mode 1 assures negative stiffness to be lower than the positive stiffness (stage flexures). As such, the negative stiffness acts around a stable equilibrium position and bistability or a constant force offset is avoided. This can be easily achieved by making the negative stiffness flexure longer.

However, in some cases a force offset may be desirable. For example when the motion direction is aligned with gravity. By using an appropriately sized proof mass, a constant force offset is able to counteract the gravitational pull, allowing for low frequency oscillations in this direction. A similar approach was taken in [23].

If the induced deformation were purely elastic, each device should have been bistable, as shown in [12], [42]. However, plastic deformation in the silicon beams has caused buckling shape mode 2 to become the new neutral position. Although mono-crystalline silicon is often considered brittle, plastic deformation is known to occur [52]. Plastic deformation of the silicon most likely happens during cool down between approximately 630 °C and 970 °C. This region is above the brittle-to-ductile transition temperature of silicon [53] and below the viscous flow point of silicon dioxide [54], [55]. However, we have no data to confirm this.

Simulations of the unbalanced stages are in good agreement with measurements. Simulations of the balanced stages model the general behaviour, however there is discrepancy in the force offset. The discrepancy may be explained by violation of the assumption that the permanently deformed shape is stress free. Indeed stress is relieved due to plastic deformation, however only those that exceed the yield stress. Stress just below the yield stress will still be present. Properly modeling this phenomenon requires implementation of constitutive models for the elasto-viscoplastic behaviour of mono-crystalline silicon, such as [53], [56], [57].

Alternatively one may work with thin films below the brittle-to-ductile transition temperature of silicon to prevent plastic deformation. Here we are not limited to thermally grown SiO_2, because Si3Ni4 (plasma 50 kHz at 350 °C and poly Si (LPCVD between 560 °C and 670 °C are reported to contain residual compressive stress between -0.1 GPa and -2.1 GPa [58]. It can even be argued that static balance can be achieved with residual tensile film stress, because a mechanisms that buckles under tensile dead load is reported in [59].

We have improved upon the state of the art [19]–[21], by investigating a versatile permanent preloading method for micro compliant mechanisms. Our method enables static balancing of mechanisms by stretching micro beams. By using the balancing structure as an isolated building block, it should be able to permanently reduce stiffness in existing mechanisms such as shown in [26].

The method is suited for massive parallelized fabrication, since thermal oxidation of silicon is a common method in semi-conductor manufacturing. It consumes no power after manufacturing and has a low manufacturing complexity. It is able to theoretically reduce stiffness to $0\,\mathrm{N\,m^{-1}}$ [33] and has the potential to be 100% space efficient if positive and negative stiffness are united in a single structure. Our method is well suited for further miniaturization, since surface effects become predominant at smaller scales.

IX. Conclusion

In this paper we have demonstrated, for the first time, permanent stiffness reduction on micro scale suited for mass production by exploiting stress induced by thin films. A building block commonly used for stiffness reduction in large scale compliant mechanisms is made compatible with MEMS. Stiffness of a simple linear stage is reduced by a factor 9 to 46 over a range of maximally 380 µm by coupling with the balancing building block. The negative stiffness is created by stretching all beams by preloading the mono-crystalline silicon with thermally grown oxide at 1100 °C.

It can be concluded that film stress is a feasible, simple and promising permanent preloading method for permanent stiffness reduction of compliant micro mechanisms. It is completely passive, allows parallelized and low complexity manufacturing, can potentially eliminate stiffness completely, has the potential to be extremely space efficient and is scalable.

Acknowledgment

This research is conducted at the instigation of and with close collaboration of Research Institute of TAG Heuer, branch of LVMH Swiss Manufacture, La Chaux de Fonds, 2300 Switzerland, and its Director, Mr G.A.(Guy) Sémon. In addition we would like to thank Flexous B.V. and in particular Wout Ypma, Sybren Weeke and Maarten Lustig for their constructive feedback and advice, many discussions and making their measurement setup available. We would also like to thank Else Kooi Laboratory, in particular Jia Wei, for manufacturing.

References

[1] S. Kota, J. Joo, Z. Li, S. M. Rodgers, and J. Sniegowski, "Design of compliant mechanisms: Applications to MEMS," *Analog Integr. Circuits Signal Process.*, vol. 29, nos. 1–2, pp. 7–15, 2001.

[2] G. K. Ananthasuresh and L. L. Howell, "Mechanical design of compliant microsystems—A perspective and prospects," *J. Mech. Des.*, vol. 127, no. 4, pp. 736–738, 2005.

[3] L. L. Howell, *Compliant Mechanism*. Hoboken, NJ, USA: Wiley, 2001.

[4] J. A. Gallego and J. L. Herder, "Criteria for the static balancing of compliant mechanisms," in *Proc. ASME IDETC CIE*, 2010, pp. 465–473.

[5] N. Tolou, V. A. Henneken, and J. L. Herder, "Statically balanced compliant micro mechanisms (SB-MEMS): Concepts and simulation," in *Proc. ASME IDETC CIE*. New York, NY, USA: American Society of Mechanical Engineers, 2010, pp. 447–454.

[6] N. Tolou, J. A. Gallego, and J. L. Herder, "Statically balanced compliant micro mechanisms (SB-MEMS): A breakthrough in precision engineering," *Mikroniek*, vol. 50, no. 6, pp. 20–25, 2010.

[7] M. L. de Laat, H. H. P. Garza, J. L. Herder, and M. K. Ghatkesar, "A review on *in situ* stiffness adjustment methods in MEMS," *J. Micromech. Microeng.*, vol. 26, no. 6, 2016, Art. no. 063001.

[8] J. L. Herder, "Design of spring force compensation systems," *Mech. Mach. Theory*, vol. 33, nos. 1–2, pp. 151–161, 1998.

[9] S.-T. Park and T.-T. Luu, "Techniques for optimizing parameters of negative stiffness," *Proc. Inst. Mech. Eng., C, J. Mech. Eng. Sci.*, vol. 221, no. 5, pp. 505–510, 2007.

[10] J. van Eijk and J. F. Dijksman, "Plate spring mechanism with constant negative stiffness," *Mechanism Mach. Theory*, vol. 14, no. 1, pp. 1–9, 1979.

[11] D. L. Platus, "Negative-stiffness-mechanism vibration isolation systems," *Proc. SPIE*, vol. 1619, pp. 44–54, Feb. 1992.

[12] J. F. Dijksman, "A study of some aspects of the mechanical behaviour of cross-spring pivots and plate spring mechanisms with negative stiffness," Ph.D. dissertation, Delft Univ. Technol., Delft, The Netherlands, 1979.

[13] M. Schenk and S. D. Guest, "On zero stiffness," *Proc. Inst. Mech. Eng., C, J. Mech. Eng. Sci.*, vol. 228, no. 10, pp. 1701–1714, 2013.

[14] L. Berntsen, D. H. Gosenshuis, and J. L. Herder, "Design of a compliant monolithic internally statically balanced four-bar mechanism," in *Proc. ASME Int. Design Eng. Tech. Conf. Comput. Inf. Eng. Conf.* New York, NY, USA: American Society of Mechanical Engineers, 2014, Art. no. V05AT08A040.

[15] K. Hoetmer, J. L. Herder, and C. J. Kim, "A building block approach for the design of statically balanced compliant mechanisms," in *Proc. ASME IDETC CIE*. New York, NY, USA: American Society of Mechanical Engineers, 2009, pp. 313–323.

[16] J. Lassooij, N. Tolou, G. Tortora, S. Caccavaro, A. Menciassi, and J. Herder, "A statically balanced and bi-stable compliant end effector combined with a laparoscopic 2DoF robotic arm," *Mech. Sci.*, vol. 3, no. 2, pp. 85–93, 2012.

[17] F. M. Morsch and J. L. Herder, "Design of a generic zero stiffness compliant joint," in *Proc. ASME IDETC CIE*. New York, NY, USA: American Society of Mechanical Engineers, 2010, pp. 427–435.

[18] L. C. Leishman, D. J. Ricks, and M. B. Colton, "Design and evaluation of statically balanced compliant mechanisms for haptic interfaces," in *Proc. ASME DSCC*. New York, NY, USA: American Society of Mechanical Engineers, 2010, pp. 859–866.

[19] P. J. Pluimers, N. Tolou, B. D. Jensen, L. L. Howell, and J. L. Herder, "A compliant on/off connection mechanism for preloading statically balanced compliant mechanisms," in *Proc. ASME IDETC CIE*. New York, NY, USA: American Society of Mechanical Engineers, 2012, pp. 373–377.

[20] N. Tolou, P. Estevez, and J. L. Herder, "Collinear-type statically balanced compliant micro mechanism (SB-CMM): Experimental comparison between pre-curved and straight beams," in *Proc. ASME IDETC CIE*. New York, NY, USA: American Society of Mechanical Engineers, 2011, pp. 113–117.

[21] G. Chen and S. Zhang, "Fully-compliant statically-balanced mechanisms without prestressing assembly: Concepts and case studies," *Mech. Sci.*, vol. 2, no. 2, pp. 169–174, 2011.

[22] F. Acernese, R. De Rosa, G. Giordano, R. Romano, and F. Barone, "Tunable mechanical monolithic sensor with interferometric readout for low frequency seismic noise measurement," *Proc. SPIE*, vol. 6932, Apr. 2008, Art. no. 69320K.

[23] R. P. Middlemiss, A. Samarelli, D. J. Paul, J. Hough, S. Rowan, and G. D. Hammond, "Measurement of the Earth tides with a MEMS gravimeter," *Nature*, vol. 531, no. 1, p. 614–617, Mar. 2016.

[24] M. Han, Q. Yuan, X. Sun, and H. Zhang, "Design and fabrication of integrated magnetic MEMS energy harvester for low frequency applications," *IEEE/ASME J. Microelectromech. Syst.*, vol. 23, no. 1, pp. 204–212, Jan. 2014.

[25] Y. Naruse, N. Matsubara, K. Mabuchi, M. Izumi, and S. Suzuki, "Electrostatic micro power generation from low-frequency vibration such as human motion," *J. Micromech. Microeng.*, vol. 19, no. 9, 2009, Art. no. 094002.

[26] D. F. Machekposhti, J. L. Herder, G. Sémon, and N. Tolou, "A compliant micro frequency quadrupler transmission utilizing singularity," *J. Microelectromech. Syst.*, vol. 27, no. 3, pp. 506–512, 2018.

[27] B. J. Nelson, I. K. Kaliakatsos, and J. J. Abbott, "Microrobots for minimally invasive medicine," *Annu. Rev. Biomed. Eng.*, vol. 12, pp. 55–85, Aug. 2010.

[28] G. C. A. M. Janssen, "Stress and strain in polycrystalline thin films," *Thin Solid Films*, vol. 515, no. 17, pp. 6654–6664, 2007.

[29] M. W. Judy, Y.-H. Cho, R. T. Howe, and A. P. Pisano, "Self-adjusting microstructures (SAMS)," in *Proc. IEEE Micro Electro Mech. Syst. (MEMS)*, Jan. 1991, pp. 51–56.

[30] M. J. Lachut and J. E. Sader, "Effect of surface stress on the stiffness of cantilever plates," *Phys. Rev. Lett.*, vol. 99, no. 20, 2007, Art. no. 206102.

[31] M. J. Lachut and J. E. Sader, "Effect of surface stress on the stiffness of thin elastic plates and beams," *Phys. Rev. B, Condens. Matter*, vol. 85, no. 8, 2012, Art. no. 085440.

[32] R. B. Karabalin, L. G. Villanueva, M. H. Matheny, J. E. Sader, and M. L. Roukes, "Stress-induced variations in the stiffness of micro- and nanocantilever beams," *Phys. Rev. Lett.*, vol. 108, no. 23, 2012, Art. no. 236101.

[33] M. I. Younis, *MEMS Linear and Nonlinear Statics and Dynamics*, vol. 20. New York, NY, USA: Springer, 2011.

[34] M. Ohring, *Materials Science of Thin Films*. New York, NY, USA: Academic, 2001.

[35] J. A. Thornton and D. W. Hoffman, "Stress-related effects in thin films," *Thin Solid Films*, vol. 171, no. 1, pp. 5–31, 1989.

[36] M. F. Doerner and W. D. Nix, "Stresses and deformation processes in thin films on substrates," *Crit. Rev. Solid State Mater. Sci.*, vol. 14, no. 3, pp. 225–268, 1988.

[37] D. Hoffman and J. A. Thornton, "Internal stresses in Cr, Mo, Ta, and Pt films deposited by sputtering from a planar magnetron source," *J. Vac. Sci. Technol.*, vol. 20, no. 3, pp. 355–358, 1982.

[38] F. J. Shaker, "Effect of axial load on mode shapes and frequencies of beams," Lewis Res. Center, NASA, Cleveland, OH, USA, Tech. Rep. TN D-8109, 1975.

[39] A. Bokaian, "Natural frequencies of beams under compressive axial loads," *J. Sound Vib.*, vol. 126, no. 1, pp. 49–65, 1988.

[40] H. Guckel, T. Randazzo, and D. W. Burns, "A simple technique for the determination of mechanical strain in thin films with applications to polysilicon," *J. Appl. Phys.*, vol. 57, no. 5, pp. 1671–1675, 1985.

[41] M. A. Hopcroft, W. D. Nix, and T. W. Kenny, "What is the Young's modulus of silicon?" *J. Microelectromech. Syst.*, vol. 19, no. 2, pp. 229–238, Apr. 2010.

[42] J. Qiu, J. H. Lang, and A. H. Slocum, "A curved-beam bistable mechanism," *J. Microelectromech. Syst.*, vol. 13, no. 2, pp. 137–146, Apr. 2004.

[43] D. M. Brouwer, J. P. Meijaard, and J. B. Jonker, "Large deflection stiffness analysis of parallel prismatic leaf-spring flexures," *Precis. Eng.*, vol. 37, no. 3, pp. 505–521, 2013.

[44] B. E. Deal and A. S. Grove, "General relationship for the thermal oxidation of silicon," *J. Appl. Phys.*, vol. 36, no. 12, pp. 3770–3778, 1965.

[45] Y. Okada and Y. Tokumaru, "Precise determination of lattice parameter and thermal expansion coefficient of silicon between 300 and 1500 K," *J. Appl. Phys.*, vol. 56, no. 2, pp. 314–320, 1984.

[46] F. Maseeh, M. Arnone, and S. D. Senturia, "Mechanical properties of microelectronics thin films: Silicon dioxide (SiO_2)," MIT, Cambridge, MA, USA, Tech. Rep. 89-575, 1989.

[47] H. Tada *et al.*, "Thermal expansion coefficient of polycrystalline silicon and silicon dioxide thin films at high temperatures," *J. Appl. Phys.*, vol. 87, no. 9, pp. 4189–4193, 2000.

[48] G. Carlotti, L. Doucet, and M. Dupeux, "Comparative study of the elastic properties of silicate glass films grown by plasma enhanced chemical vapor deposition," *J. Vac. Sci. Technol. B, Microelectron. Nanometer Struct. Process., Meas., Phenomena*, vol. 14, no. 6, pp. 3460–3464, 1996.

[49] J.-H. Zhao, T. Ryan, P. S. Ho, A. J. McKerrow, and W.-Y. Shih, "Measurement of elastic modulus, Poisson ratio, and coefficient of thermal expansion of on-wafer submicron films," *J. Appl. Phys.*, vol. 85, no. 9, pp. 6421–6424, 1999.

[50] D.-B. Kao, J. P. McVittie, W. D. Nix, and K. C. Saraswat, "Two-dimensional thermal oxidation of silicon—I. Experiments," *IEEE Trans. Electron Devices*, vol. 34, no. 5, pp. 1008–1017, May 1987.

[51] Q. Xu, "Design of a large-stroke bistable mechanism for the application in constant-force micropositioning stage," *J. Mech. Robot.*, vol. 9, no. 1, 2017, Art. no. 011006.

[52] J. Kim, H. Choo, L. Lin, and R. S. Muller, "Microfabricated torsional actuators using self-aligned plastic deformation of silicon," *J. Microelectromech. Syst.*, vol. 15, no. 3, pp. 553–562, Jun. 2006.
[53] H.-S. Moon, L. Anand, and S. M. Spearing, "A constitutive model for the mechanical behavior of single crystal silicon at elevated temperature," in *Proc. Mater. Res. Soc. Symp.*, vol. 687, 2002, Paper B9.6.1.
[54] E. P. EerNisse, "Viscous flow of thermal SiO_2," *Appl. Phys. Lett.*, vol. 30, no. 6, pp. 290–293, 1977.
[55] E. P. EerNisse, "Stress in thermal SiO_2 during growth," *Appl. Phys. Lett.*, vol. 35, no. 1, pp. 8–10, 1979.
[56] J. Cochard, I. Yonenaga, S. Gouttebroze, M. M'Hamdi, and Z. Zhang, "Constitutive modelling of silicon: Parameters identification of classical models using crystal plasticity," in *Proc. 3rd Int. Workshop Crystalline Silicon Solar Cells*. Trondheim, Norway: SINTEF/NTNU, Jun. 2009.
[57] J. Cochard, I. Yonenaga, S. Gouttebroze, M. M'Hamdi, and Z. Zhang, "Constitutive modeling of intrinsic silicon monocrystals in easy glide," *J. Appl. Phys.*, vol. 107, no. 3, 2010, Art. no. 033512.
[58] S. M. Hu, "Stress-related problems in silicon technology," *J. Appl. Phys.*, vol. 70, no. 6, pp. R53–R80, 1991.
[59] D. Zaccaria, D. Bigoni, G. Noselli, and D. Misseroni, "Structures buckling under tensile dead load," *Proc. Roy. Soc. A, Math., Phys. Eng. Sci.*, vol. 467, pp. 1686–1700, Jan. 2011.

P. Reinier Kuppens received the M.Sc. degree *(cum laude)* in mechanical engineering from the Delft University of Technology, Delft, The Netherlands, in 2016. He is currently pursuing the Ph.D. degree in mechanical engineering with the Department of Precision and Microsystems Engineering, Delft University of Technology. His primary research interest is in the design, analysis, and manufacturing of small scale spring mechanisms with low stiffness.

Just L. Herder (M'06) received the M.Sc. and Ph.D. degrees in mechanical engineering from the Delft University of Technology, Delft, The Netherlands, in 1992 and 2001, respectively. He held visiting positions at Laval University, Canada, and at MIT, USA, as a Fulbright Visiting Scholar. He is currently a Full Professor and the Head of the Department of Precision and Microsystems Engineering, Delft University of Technology, Delft. He has published over 280 publications in international peer reviewed journals and conferences and gave over a dozen keynote talks at international conferences. He holds 25 patents in different areas of mechanism design, based on which seven start-up companies have emerged. He is a Fellow of the ASME. He received the several international awards, including six best paper awards. He is an Associate Editor of the Mechanism and Machine Theory, a founding Editor-in-Chief of Mechanical Sciences, and an Organizer of several international conferences.

Nima Tolou received the Ph.D. degree from the Department of Biomechanical Engineering, Delft University of Technology, The Netherlands, in 2012. He was a Visiting Scholar with Brigham Young University, Provo, UT, USA, from 2011 to 2012, and a Marie Curie Fellow with the Department of Electrical and Electronic Engineering, Imperial College London, U.K., from 2013 to 2014. Since 2014, he has been an Assistant Professor with the Delft University of Technology. His current research focus is on design of precision MEMS and micro motion energy harvesters for medical applications and high-tech industry.